Detection and Aggregation of the Antitumoral Drug Parietin in Ethanol/Water Mixture and on Plasmonic Metal Nanoparticles Studied by Surface-Enhanced Optical Spectroscopy: Effect of pH and Ethanol Concentration

Eduardo Lopez-Tobar[a], Valeria Verebova[b], Ludmila Blascakova[c], Daniel Jancura[c,d], Gabriela Fabriciova[c], Santiago Sanchez-Cortes[a]*

[a]*Instituto de Estructura de la Materia. IEM-CSIC. Serrano, 121. 28006 Madrid, Spain.*

[b]*University of Veterinary Medicine and Pharmacy, Komenskeho 73, 041 81 Kosice, Slovak Republic.*

[c]*Department of Biophysics, P.J. Safarik University in Kosice, Jesenna 5, 041 54 Kosice, Slovak Republic.*

[d]*Center for Interdisciplinary Biosciences, P.J. Safarik University in Kosice, Jesenna 5, 041 54 Kosice, Slovak Republic.*

**Corresponding Author*

E-mail: s.sanchez.cortes@csic.es

Abstract

In the present paper, we have investigated the effect of ethanol in aqueous media, the pH and the presence of Ag nanoparticles (NPs) on the aggregation processes of the antitumoral anthraquinone parietin in aqueous media and on the metal surface. UV-visible absorption, fluorescence and Raman spectra of parietin were used for such purpose. The present study provides information about the deprotonation and molecular aggregation processes occurring in parietin under different environments: ethanol/water mixture and when adsorbed onto Ag nanoparticles. The effect of ethanol on the optical properties of parietin in alcohol-water mixtures was also investigated at different ethanol concentrations with the time. For the case of the adsorption and organization of parietin molecules on the surface of Ag NPs, special attention was paid to the use of surface-enhanced optical techniques SEF (surface-enhanced fluorescence) and SERS (surface-enhanced Raman scattering) for the characterization of the parietin aggregates and the ionization of the molecule on the surface. In particular, we have studied the variation of the SEF signal with the pH, which depends on the molecular organization of the molecule on the surface. Furthermore, a detailed analysis of the SERS spectra at different pH was accomplished and the main Raman bands of the protonated, mono-deprotonated and di-deprotonated parietin were identified. Finally, the second ionization pK of parietin on metal NPs was deduced from the SERS spectra.

Keywords: parietin, fluorescence, surface-enhanced Raman spectroscopy (SERS), surface-enhanced Fluorescence (SEF), aggregation, adsorption.

1 Introduction

The anthraquinone parietin (1,8-dihydroxy-3-methoxy-6-methylanthraquinone) (Fig. 1) is an orange pigment found in lichens of the families *Teloschistaceae, Brigantiaceae, Letroutiaceae* and *Psoraceae* [1-3]. In addition, parietin can be also found in plants of the genus *Rhamnus* and *Rheum*. This pigment is deposited mostly on the surface of mycobiont *hyphae* in the cortical layer of stratified lichen *thalli*. It is proposed that synthesis of parietin in lichens is induced by UV-B [4] and stimulated by photosynthesis [5]. Parietin protects lichen photobiont cells against excessive photosynthetically active light [1,6-9]. The mechanism for the light screening by parietin is based on a high absorption of the solar radiation in the 400-500 nm region, which is one of the most important active region in the photosynthesis [10]. In addition, parietin possesses some important biological activities, including antibacterial and antifungal effects [11,13]. However, the main interest of parietin in recent years was based on the ability of this pigment to inhibit the proliferation of cancerous cell and the fact that it can induce apoptosis in various types of human cancer cells [14]. The mechanism of action of parietin was very recently unveiled and it was shown to be related to its ability to inhibit the gluocose-6-phosphate dehydrogenase (G6PD), the first enzyme of the oxidative pentose phosphate pathway (PPP), that produces nicotinamide adenine dinucleotide phosphate (NADPH): This effect results in attenuated cell growth with potentiated H_2O_2-mediated cell death, probably due to lack of NADPH [15].

The structure of parietin has been investigated by NMR spectroscopy [16], mass spectrometry [17], FT-Raman and infrared spectroscopy [18]. The high fluorescence emission of this anthraquinone avoids the application of classical Raman spectroscopy to study the vibrational properties of parietin in solution. In a previous work, we have applied FT-Raman, surface-enhanced Raman spectroscopy (SERS), and DFT

calculations for the elucidation of the vibrational properties of this molecule [19]. We have demonstrated that SERS is a valid method to study the behavior of this molecule in solutions. Moreover, the adsorption mechanism of parietin towards surface of silver nanoparticles was proposed.

In the present paper, we have investigated the effect of ethanol in aqueous media, the pH and the presence of Ag nanoparticles on the aggregation processes of parietin in aqueous media and on the metal surface. UV-visible absorption, fluorescence and Raman spectra of parietin were used to investigate the adsorption on NPs and for the detection of low concentrations of the different molecular forms of this molecule. Special attention was paid to the use of fluorescence and SEF (surface-enhanced fluorescence) for the characterization of the parietin aggregates. The present study also provides information about the deprotonation and molecular aggregation processes occurring in parietin under different environments: ethanol/water mixture and when adsorbed onto Ag nanoparticles. An analysis of the pH dependence of parietin SERS and SEF spectra, including the SERS spectral markers for the protonated, mono-deprotonated and di-deprotonated parietin, is also presented that affords a comprehensive information about the different molecular forms of this antitumoral natural drug.

The fluorescence of anthraquinone molecules is very high in organic solvents where they are very well solubilized as it was already demonstrated for related hydroxyquinone molecules such as hypericin [20]. However, the situation is very different in water, where anthraquinone molecules tend to be aggregated, and their fluorescence is almost vanished due to the quenching effect of intermolecular stacking existing in aggregates [21,22]. This is a drawback that can affect seriously the biological activity of these molecules. The aggregation capability of anthraquinones in aqueous

media can be modified by changing the pH, and by the presence of organic solvents in aqueous solutions [23]. In particular, the effect of ethanol in the aggregation-disaggregation processes followed by molecules in ethanol/water mixtures is an important issue that deserves a high attention due to the special behavior of alcohols in water [24-26], and this effect was not sufficiently investigated so far.

Another interesting issue is the effect of plasmonic metal nanoparticles (NPs) on the aggregation of anthaquinone molecules due to their adsorption on the metallic surface. In our recent works it was reported that the presence of NPs can dramatically affect the aggregation capability of anthraquinone molecules [22,23]. It was shown that the intensity of the Raman and fluorescence spectra of adsorbed anthraquinones can be highly enhanced in the presence of NPs due to the existence of localized surface plasmon resonance (LSPR) on the surface of NPs. This phenomenon allows the study of the vibrational properties of these molecules at low concentrations on the interface, while the enhancement of the fluorescence of anthraquinone aggregates can provide valuable information about these aggregation processes occurring on the surface. The present paper has two objectives that clearly justify the development of such an investigation: a) the possibility of having a simultaneous enhancement of both the Raman and fluorescence signals from these molecules at trace concentrations, and b) the detection of a fluorescence signal from anthraquinone aggregates. In consequence, vibrational and electronic information from the same system can be obtained at the same conditions and a more complete characterization of the aggregation processes of parietin is then possible. The study of this aggregation is of a high importance to evaluate the biological activity and the availability of this antitumoral drug in aqueous media.

2 Material and methods

2.1 Reagents

Parietin was obtained from two different sources: natural and commercial. The natural parietin was extracted from the lichen *Xanthoria parietina* by following the protocols of Solhaug and Gauslaa [1]. Crystals of the compounds were finally dissolved in pure acetone and recrystallized. The identity and purity of the compounds was assessed using TLC and HPLC analyses. The commercial parietin was purchased from Sigma-Aldrich. For both types of the samples the vibrational data were very similar in all experiments. Thus, we only show those obtained using the commercial parietin. Potassium nitrate, hydroxylamine hydrochloride, sodium hydroxide, nitric acid, hydrochloric acid, sodium bicarbonate, potassium hydrogen phthalate, potassium dihydrogen phosphate, and Tris (Tris(hydroxymethyl)aminomethane) were purchased from Sigma-Aldrich and silver nitrate was obtained from Merck. All reagents used were of analytical grade. Milli-Q water was used to dissolve all reagents and a stock solution of parietin was prepared in absolute ethanol (99.5 % purity, Merck). The solutions of ethanol/water were prepared by mixing variable volumes of each solvent and the concentration is expressed as ethanol percent in v/v.

2.2 Preparation of silver colloid

Ag NPs (SHAg) were prepared by chemical reduction silver nitrate with hydroxylamine hydrochloride by the method described previously [27]. A total of 300 μL of a sodium hydroxide solution (1 M) was added to 90 mL of a 1.66×10^{-3} M hydroxylamine hydrochloride aqueous solution. Then, 10 mL of a 10^{-2} M silver nitrate aqueous solution were added drop-wise to the mixture under vigorous stirring. Finally a brown silver colloid was obtained with a final pH 5.5. This process was carried out under room temperature.

2.3 Surface-enhanced Raman spectroscopic measurements

Samples for SEF and SERS experiments were prepared by previously activating the Ag colloid with 0.5 M KNO_3. The activation at alkaline or acidic pH was accomplished by adding 0.25 M, 1 M or 2 M NaOH and 0.2 M HNO_3 aqueous solutions. The ratio of these activators depended on the final pH. The total volume of the activator was 30 μL, which was added to 1 mL of the colloid. Then, 10 μL of a stock solution of parietin in ethanol was added to 990 μL activated colloid. The final concentrations of parietin in the sample were 10^{-5}, 7×10^{-6} and 5×10^{-7} M and that of ethanol was 1%. In the case of experiments in water solution carried out in absence of Ag NPs, the preparation method was the same, although Milli-Q water was used instead of the Ag colloid. The standard deviation of the SERS intensities was approximately 10% thus demonstrating a relatively high level of reproducibility.

FT Raman spectra were obtained by using a MultiRam Bruker spectrometer equipped with a high-sensitivity Ge diode detector. The 1064 nm line provide by a air cooled Nd^{3+}:YAG laser source (1064 nm). The laser power was 200 mW and 400 mW in solid sample and solution respectively and the resolution was set to 4 cm^{-1}. The Raman spectra in this work are the result of 200 and 1000 accumulations average.

The SERS spectra were collected with a Renishaw Raman Invia Spectrometer ,equipped with a CCD camera, at 442nm (He:Cd) and 532 nm (Nd:YAG) lines lasers. The output laser power was fixed at 30 mW, 50 mW respectively, which corresponds to 3 mW, 8 mW and 18mW on the sample. The resolution was set 2 cm^{-1} and one scan of 10 seconds was recorded in each of them.

2.4 Fluorescence and UV–vis absorbance spectra

UV–vis absorption and fluorescence spectroscopy measurements were carried out in the 8.0–12.0 pH range and final concentration of parietin was 7.5×10^{-6} M. These

samples contained 5% of ethanol, and were prepared in KDP buffer solution (0.1 M KH_2PO_4, 0.1 M NaOH: pH = 6.0–8.0), Tris-HCl buffer (0.1 M Tris, 0.1 M HCl: pH = 8.0–9.2) and bicarbonate buffering solution (0.05 M $NaHCO_3$, 0.1 M NaOH: pH = 9.4–12.0). All buffers were prepared in Milli-Q water. A SHIMADZU UV-2401 PC Spectrophotometer was employed to obtain the UV-vis absorption spectra. Quartz cuvette of 1 cm was used for measuring in the 350–750 nm range. Fluorescence measurements were performed by using a SHIMADZU RF-5301 PC spectrofluorimeter. The excitation wavelength was fixed at 434 nm and the emission spectra were recorded in the 440–700 nm range. Kinetic experiments were conducted immediately after sample preparation, excitation wavelength was 434 nm and emission wavelengths were varied as a function of the maximum of the fluorescence band. The obtained absorption and fluorescence spectra were further processed and adjusted by the Origin 8.0 program. All UV-vis absorption spectra were offset in a manner that the absorbance at 700 nm is zero.

3 Results and discussion

3.1 UV–vis and fluorescence spectra of parietin in ethanol/water mixtures

Fig. 2 shows the UV-vis absorption spectra of parietin in ethanol/water mixtures at different ethanol concentrations. The visible absorption spectrum of parietin in pure ethanol is characterized by an intense broad band at 434 nm which arises from a π–π* transition [28]. An increase of a water content in the ethanol/water mixture leads to a gradual bathochromic shift of the band with maximum at 434 nm to a band at 442 nm (inset figure). This behavior is observed up to 20% ethanol in water. Below this ethanol concentration, a hypsochromic shift of this band to 421 nm is observed. The strong decrease of the absorption intensity of parietin at low ethanol concentrations is related

mainly to the formation of parietin aggregates, which is characteristic also for other anthraquinone molecules in aqueous media [20-22].

The fluorescence emission spectrum of parietin in pure ethanol (Fig. 3a) shows an intense band at 509 nm with a shoulder at 530 nm. As the amount of water is increased in the ethanol/water mixture, a progressive shift of the emission band to higher wavelengths is observed (Fig. 3c). This effect is associated with the increase of the solvent polarity [29]. In addition, the intensity of the fluorescence emission of parietin undergoes a remarkable decrease on lowering the ethanol content (Fig. 3b). The quenching is mainly evident at ethanol concentrations below 20-25%, reaching an almost negligible value in pure water. This effect is again attributed to the parietin aggregation undergone in aqueous medium. Fig. 3b shows that the intensity of the fluorescence emission from parietin decreases as the ethanol content is lowered in a sigmoidal manner and it becomes very low below 20%. A similar aggregation effect was also reported for other anthaquinones such as hypericin [30] and emodin [23], and this behavior is often connected with the loss of the biological activity of this type of molecules [31]. This loss is due to a significant decrease of the quantum yields of singlet oxygen formation and fluorescence [32].

The optical properties of parietin (UV–vis absorption and fluorescence) in ethanol/water mixture can be explained on the basis of the different organization of water and ethanol molecules in the solution at different ethanol content [24-26] and the unusual packing propensity of ethanol in aqueous solution. At concentration of ethanol 20%, it was reported that the ethanol/water system reaches the highest degree of structuring of the hydrogen bond network, which corresponds to the slowest translational dynamics within mixture [26]. However, at higher concentration of ethanol, a gradual increase in diffusivity was reported to occur [25]. Below 20%, the

ethanol/water interactions are influenced by the formation of cage-like structures also called “icebergs”, while at higher concentrations, the formation of chains or rings of ethanol dictates packing characteristics [22]. This behavior creates inhomogeneties in the alcohol-water system that provokes the formation of an actual biphasic system, where the solute molecules can diffuse from one phase to another. At ethanol contents below 20%, this biphasic model starts to be disrupted and the amount of single ethanol molecules increases [26].

The aggregation of parietin in an ethanol/water mixture also follows a time evolution (Fig. 3d) at intermediate ethanol concentrations (10–35%), which implies a substantial fluorescence decrease. This quenching effect is very slow at ethanol concentrations above 20% and very fast at ethanol contents below this value. This behavior is associated with the existence of inhomogeneties in the alcohol/water system due to the formation of clusters of alcohol molecules [26] that leads to the formation of an actual biphasic system, where the solute molecules can diffuse from one phase (ethanol) to the other (water). Under these conditions, at the intermediate concentrations of ethanol (10–40%), parietin seems to be solved in the ethanolic phase immediately after its addition to the mixture. Afterwards, the anthraquinone diffuses to the aqueous part giving rise to aggregates that are responsible for the fluorescence quenching with time. This process is also favored by the formation of parietin aggregates in the water environment.

Above 35% of ethanol, the fluorescence intensity of parietin practically does not undergo any change with time. This is attributed to the fact that immediately after parietin incorporation into the ethanol/water mixture, the molecules of parietin are completely solved in the organic phase and no diffusion to the aqueous part occurs [26]. At these conditions, parietin exists in a monomeric state and emits an intense

fluorescence signal. The intensity of parietin fluorescence does not exhibit any time dependence also in the situation when the concentration of ethanol is very low (Fig. 3d). In this case, most of the parietin molecules remain in the aqueous phase of the mixture where they form aggregates.

3.2 pK value for parietin

The UV–vis absorption spectra of parietin in aqueous solution (5% in ethanol) at different pH are shown in Fig. 4. As it can be seen, the absorption spectrum of parietin is very sensitive to the variation of pH. The absorption band changes its maximum from 422 nm to 504 nm when the pH varies from 7 to 12 and the color of the solution changes from yellow to red. At pH lower than 7, the parietin aggregation and precipitation in water excludes recording the absorption spectrum. The absorption maxima at 422 and 504 nm correspond to two different parietin forms: monoanionic and dianionic (Fig. 1). The pKa_2 value of 9.8 ± 0.1 corresponding to the dissociation of parietin monoanionic form was deduced from the titration curve shown in insert of Fig. 4. The difference from the values reported previously for this pKa_2 (8.58) [33] is attributed to the different solvent conditions and also the different solvent-water ratio. On the other hand, this pKa_2 is close to the pKa value obtained for another anthraquinone molecule danthron (9.5) [34]. The pKa_1 could not be obtained because of the strong aggregation of parietin at low pH. However, the dissociation constant pKa_1 was determined in methanol by UV–vis spectroscopy [35] and the value is 3.9.

3.3 Surface-Enhanced fluorescence and Raman of parietin on Ag nanoparticles

The adsorption of anthraquinones on Ag NPs leads to a dramatic change of the optical properties of these molecules that induces a strong enhancement of the intensity of both the fluorescence and the Raman spectra. Parietin is able to approach the metal surface giving rise to surface-enhanced fluorescence and Raman spectra which intensity

depends on the organization of the molecule on the surface of nanoparticles, since the SEF and SERS effects highly depend on the distance of the molecule to the surface [22]. Indeed, the pH has an important effect on the molecular organization on the surface. Fig. 5B shows the surface-enhanced optical (fluorescence + Raman) spectra obtained for parietin at different conditions. This figure contains also a pH dependence of the parietin fluorescence emission at 594 nm (corresponding to 5800 cm^{-1} at 442 nm excitation) at two different concentrations on Ag NPs (circles) and in water (stars). It is observed that the fluorescence intensity becomes stronger on Ag NPs at acidic pH. This effect is attributed to the formation of parietin aggregates on the surface at low pH as indicated in Fig. 5A, and this aggregate formation is more pronounced at higher parietin concentration (dark circles). The presence of these aggregates allows the existence of parietin molecules at distances for which a surface-enhanced fluorescence (SEF) emission occurs. Thus, on Ag NPs the emission undergoes an opposite behavior regarding that seen in aqueous solution in the sense that the aggregation enhances the emission of fluorescence, while in solution this aggregation causes the fluorescence quenching. This opposite behavior is also translated to the alkaline pH, since the fluorescence emission strongly decreases due to the interaction of monomeric parietin molecules with the metal surface that induces a subsequent fluorescence quenching through an energy transfer mechanism.

3.4 Effect of pH on the Surface-enhanced Raman spectrum of parietin

Fig. 6 shows the SERS spectra of parietin at different pH using excitation line at 442 nm together with the FT-Raman (excitation at 1064 nm) spectrum of this compound in powder. At pH 2.5 (Fig. 6b) the SERS spectrum is dominated by intense bands at 1675, 1555, 1367, 1278, 925 and 461 cm^{-1}, which are only slightly shifted in comparison to the FT-Raman spectrum of the solid parietin (Fig. 6a). This similarity

suggests that at low pH the molecules of parietin are adsorbed on Ag nanoparticles under the neutral form, which exists in the solid state. But there are differences concerning bands attributed to the vibrations of hydroxyl and keto groups (see for instance the bands at 1613 and 1278 cm^{-1}), which can be due to the different excitation wavelengths (442 nm vs. 1064 nm) and also a different arrangement of the molecule on the metal surface. The SERS spectra at pH 2.5, 6.0 and 12.0 are clearly different (Fig. 6 b, d, and f), therefore we assume that parietin can exist in the 2.5 – 12 pH interval under three different forms: neutral, monanionic and dianionic as indicated in the inset structures in Fig. 6. The excitation at 442 nm induces the pre-resonance Raman scattering of the neutral and monanionic forms (Fig. 4), while the excitation at 532 nm is resonant for the dianionic form, although this can change when these molecules are adsorbed on the surface of NPs.

In going from the acidic to neutral and alkaline pH remarkable changes are observed in the SERS spectra of parietin. The band appearing in the SERS spectrum in the acidic conditions at 1674 cm^{-1} (Fig. 6a) disappears at both neutral (Fig. 6c-e) and basic pH (Fig. 6f), while other bands appear at 1644 cm^{-1} and 1337 cm^{-1} and their intensities increase with the pH. In addition, the band appearing at 1555 cm^{-1} is upward shifted to 1564 cm^{-1} and the bands at 1367 and 1278 cm^{-1} are markedly weakened going from acidic to basic pH. All these changes are related to molecular deprotonation, since they involve bands attributed to C-OH and C=O stretching or O-H bending motions, which are sensitive to the internal H-bonds established with the vicinal C=O group, as indicated by theoretical calculation [19]. The band at 1675 cm^{-1}, only seen at acidic conditions, may be assigned to the ν(C=O). This band is stable in emodin, molecule structurally very similar to parietin, until alkaline pH [23]. This is due to the fact that in emodin the first deprotonation occurs on the OH at position 3. Thus, the deprotonation

of OH groups adjacent to the carbonyl group in parietin is the responsible for the SERS spectral changes observed from acidic to neutral pH. Moreover, the changes observed at alkaline pH are ascribed to the second deprotonation. These second ionization leads to the disappearance of bands at 1617 and 1593 cm^{-1}, and the large weakening of the bands associated with double bonds due to the resonance loss caused by the absorption maximum shift to higher wavelengths. Therefore, the latter changes allowed us to assign the SERS spectra corresponding to the neutral, monoionized and dianionic form of parietin that can be seen in Fig. 6. The strong band at 1647 cm^{-1} is assigned to the carbonyl group in position 9, which is the group through which the interaction with Ag seems to take place.

The SERS spectra of parietin at different pH were also recorded at 532 nm excitation (Fig. 7). In this case, the SERS intensity markedly increases when passing from pH 8 to 12 (Fig. 7c and 7d) due to the higher resonance Raman effect of dianionic parietin at 532 nm. In general, the main part of the changes observed in the SERS spectra in going to high pH obtained at 532 nm and 442 nm are similar, although at 532 nm the band at 1340 cm^{-1} undergoes a relative stronger intensification at alkaline pH, because of the high electronic coupling between the ionized OH groups and the aromatic structure. The changes occurring in the 1700–1200 cm^{-1} region can be attributed to the ionization of OH groups of parietin. This ionization can also affect the carbonyl group in position 9, since the bands attributed to these groups are sensitive to changes of pH, due to the fact that carbonyl group is involved in internal H-bond interactions with –OH groups.

The pK_{a2} constant of parietin on Ag NPs can be deduced from the SERS spectra recorded at different pH (Fig. 7 insert) by exciting at 532 nm. To accomplish that, we have analyzed the relative intensities of the bands appearing in the 1550-1620 cm^{-1} and

the 1300-1350 cm^{-1} regions. In the insert of the Fig. 7, the intensity ratio of the bands appearing in these regions is plotted against the pH. From this plot the ionization constant of parietin on Ag NPs can be deduced, being pK_{a2} = 8.8. This pK_{a2} constant is lower as that one obtained by UV-vis measurements (pK_{a2} = 9.5). This difference is attributed to the different chemical conditions existing on the metal surface in comparison to the solution, and to the interaction of the anthraquinone with the metal.

4 Conclusion.

Parietin aggregation in aqueous solutions leads to a substantial decrease of its UV–vis absorption and fluorescence signals. This effect can be avoided by increasing the ethanol concentration in the ethanol/water mixture. However, the variation of the optical properties of parietin follows a rather complex behavior because of the special characteristics of the ethanol/water mixtures. The monomerization of parietin molecules proceeds in a sigmoidal manner with respect to the ethanol concentration in the ethanol/water mixture. Below 20% in ethanol, parietin molecules exist mostly in non-fluorescent aggregate state.

In the 20-40 % ethanol concentration range, the fluorescence of parietin also follows a time evolution which is associated with the existence of inhomogeneties in the alcohol/water system due to the formation of alcohol clusters that leads to a formation of an actual biphasic system, where the solute molecules can diffuse from one phase to the other.

The adsorption of parietin on Ag NPs leads to a remarkable enhancement of both the fluorescence and the Raman spectra. Parietin is able to approach the metal surface giving rise to an emission spectrum that can change depending on the pH. The fluorescence intensity becomes stronger on Ag NPs at acidic pH. This effect is

attributed to the formation of parietin aggregates on the metal surface which is more pronounced at higher concentration of parietin. The presence of these aggregates allows the existence of parietin molecules at distances for which a surface-enhanced fluorescence emission occurs. However, at alkaline pH the fluorescence emission strongly decreases due to the interaction of monomer parietin molecules with the metal surface that induces a subsequent fluorescence quenching through an energy transfer mechanism.

The SERS at different pH revealed the bands characteristic of the different parietin forms and allowed to follow the dissociation of the molecule on Ag NPs. The pK_{a2} deduced from the SERS spectra (pK_{a2} = 8.8) is a slightly different from that obtained in ethanol/water mixture (pK_{a2}=9.8) through UV-vis absorption measurements. This difference is mainly attributed to different chemical conditions existing on the metal surface in comparison to the solution, and to the interaction of the anthraquinone with the metal.

Acknowledgements

This work has been supported by the Spanish *Ministerio de Economía y Competitividad* (FIS2014-52212-R), by Structural funds of the EU (contracts: NanoBioSens (ITMS code: 26220220107, 50%), SEPO II (ITMS code: 26220120039), and CEVA II (ITMS code: 26220120040), by the contract APVV-0242-11, and the 7FP EU project CELIM (316310).

References

(1) K.A. Solhaug, Y. Gauslaa, Oecologia 108 (1996) 412–418.

(2) J. Hafellner, Symb. Bot. Ups. 32 (1997) 35–74.

(3) S. Johansson, U. Sochting, J.A. Elix, J.H. Wardlaw, Mycol. Prog. 4 (2005) 139–148.

(4) K.A. Solhaug, Y. Gauslaa, L. Nybakken, W. Bilger, New Phytol. 158 (2003) 91–100.

(5) K.A. Solhaug, Y. Gauslaa, Plant Cell Environ. 27 (2004) 167–176.

(6) Y. Gauslaa, K.A. Solhaug, Lichenologist 36 **(**2004) 133–143.

(7) M. McEvoy, Y. Gauslaa, K.A. Solhaug, New Phytol. 175 (2007) 271–282.

(8) M. McEvoy, K.A. Solhaug, Y. Gauslaa, Symbiosis 43 (2007) 143–150.

(9) K.A. Solhaug, P. Larsson, Y. Gauslaa, Planta 231 (2010) 1003–1011.

(10) Y. Gauslaa, E.M. Ustvedt, Photochem. Photobiol. Sci. 2 (2003) 424–432.

(11) S.K. Agarwal, S.S. Singh, S. Verma, S. Kumar, J. Ethnopharmacol. 72 (2000) 43–46.

(12) X. Ma, X. Yang, F. Zeng, L. Yang, D. Yu, H. Ni, Pest. Manag. Sci. 66 (2010) 718–724.

(13) A. Basile, D. Rigano, S. Loppi, A. Di Santi, A. Nebbioso, S. Sorbo, B. Conte, L. Paoli, F. De Ruberto, A.M. Molinari, L. Altucci, P. Bontempo, Int. J. Mol. Sci. 16 (2015) 7861–7875.

(14) M. Backorova, M. Backor, J. Mikes, R. Jendzelovsky, P. Fedorocko, Toxicol. In Vitro 25 (2011) 37–44.

(15) L. Ruiting, E. Shannon, S. Changliang et al. Nature Cell Biol. (2015) DOI: 10.1038/ncb3255

(16) M.V. Sargent, D.O.N. Smith, J.A. Elix, J. Chem. Soc. C (1970) 307–311.

(17) T.S. Wu, T.T. Jong, H.J. Tien, C.S. Kuoh, H. Furukawa, K.H. Lee, Phytochemistry 26 (1987) 1623–1625.

(18) H.G.M. Edwards, E.M. Newton, D.D. Wynn-Williams, S.R. Coombes, J. Mol. Struct. 648 (2003) 49–59.

(19) G. Fabriciova, E. Lopez-Tobar, M. V. Cañamares, M. Backor, S. Sanchez-Cortes, Vib. Spectrosc. 63 (2012) 477–484.

(20) J.L. Wynn, T.M. Cotton, J. Phys. Chem. 99 (1995) 4317–4323.

(21) T. Yamazaki, N. Ohta, I. Yamazaki, P.S. Song, J. Phys. Chem. 97 (1993) 7870–7875.

(22) G. Lajos, D. Jancura, P. Miskovsky, J.V. Garcia-Ramos, S. Sanchez-Cortes, J. Phys. Chem. C 112 (2008) 12974–12980.

(23) S. Sanchez-Cortes, D. Jancura, P. Miskovsky, A. Bertoluzza, Spectrochim. Acta A 53 (1997) 769–779.

(24) S.A. Parke, G.G. Birch, Food Chem. 67 (1999) 241–246.

(25) S.Y. Noskov, G. Lamoureux, B. Roux, J. Phys. Chem. B 109 (2005) 6705–6713.

(26) R. Li, C. D'Agostino, J. McGregor, M.D. Mantle, J.A. Zeitler, L.F. Gladden, J. Phys. Chem. B 118 (2014) 10156−10166.

(27) M.V. Cañamares, J.V. Garcia-Ramos, J.D. Gomez-Varga, C. Domingo, S. Sanchez-Cortes, Langmuir 21 (2005) 8546–8553.

(28) Z. Markovic, N. Manojlovic, S. Zlatanovic, J. Serbian Soc. Comp. Mech. 2 (2008) 73–79.

(29) J.R. Lakowicz, Principles of fluorescence spectroscopy. 3rd ed. Springer, New York (2010).

(30) S. Kascakova, M. Refregiers, D. Jancura, F. Sureau, J.C. Maurizot, P. Miskovsky, Photochem. Photobiol. 81 (2005) 1395–1403.

(31) T. Kiesslich, B. Krammer, K. Plaetzer, Curr. Med. Chem. 13 (2006) 2189–2204.

(32) P. Gbur, R. Dedic, D. Chorvat Jr., P. Miskovsky, J. Hala, D. Jancura, Photochem. Photobiol. 85 (2009) 816−823.

(33) D. Wang, G. Yang, X. Song, Electrophoresis 22 (2001) 464–469.

(34) G. Fabriciova, J.V. Garcia-Ramos, P. Miskovsky, S.Sanchez-Cortes, Vib. Spectrosc. 34 (2004) 273–281.

(35) Hauck, S.R. Jurgens, K. Willenbruch, S. Huneck, C. Leuschner, Ann. Bot. 103 (2009) 13–22.

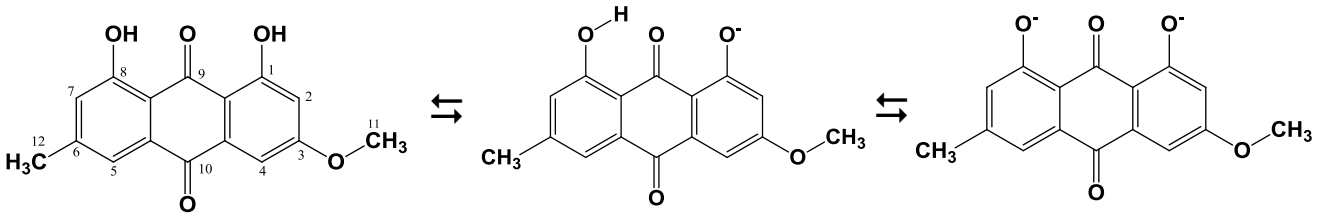

Figure 1

Parietin structure, numbering and dissociation equilibria between neutral, monoanionic and dianionic parietin forms

.

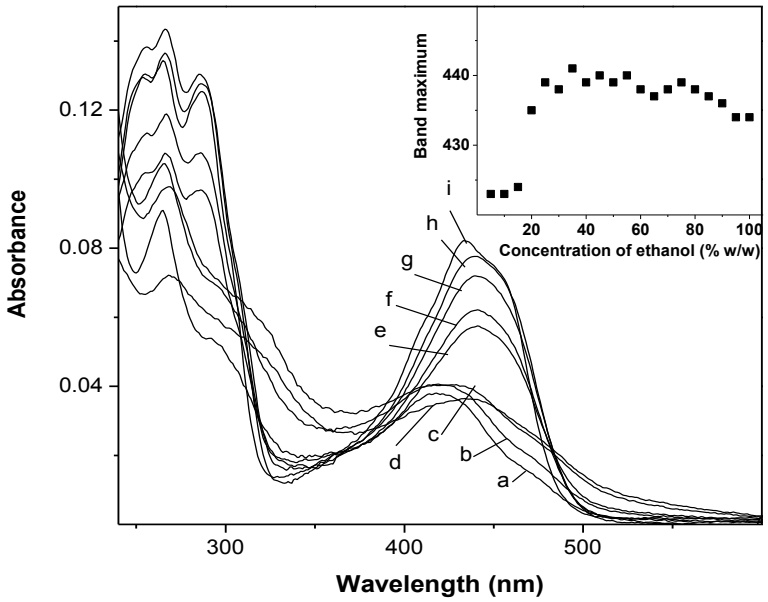

Figure 2

Effect of the ethanol concentration on the UV-vis absorption spectra of parietin (7.5 μM.) in ethanol/water mixtures: (a) 5, (b) 10, (c) 20, (d) 25, (e) 30, (f) 35, (g) 50, (h) 70, (i) 100%. Inset: effect of the ethanol concentration on the wavelength of the maximum absorbance of parietin.

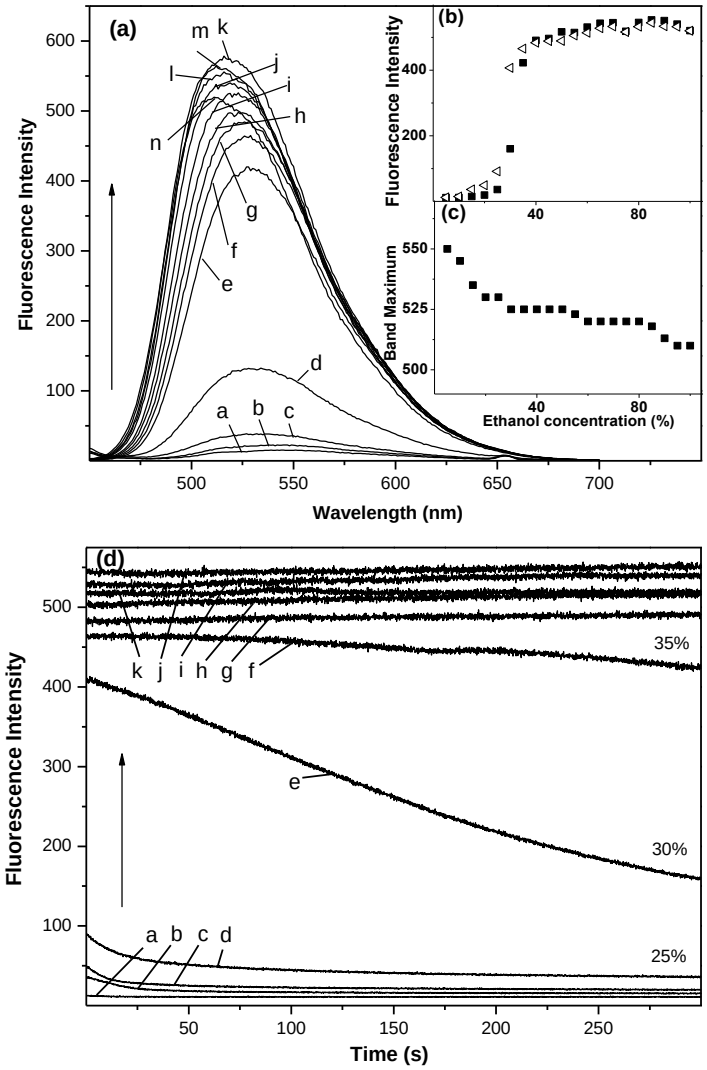

Figure 3

(a) Effect of the ethanol concentration on the fluorescence spectra of parietin (7.5 μM) in ethanol/water mixture. The ethanol concentration increases in the direction of the arrow: (a) 5, (b) 10, (c) 20, (d) 25, (e) 30, (f) 35, (g) 40, (h) 50, (i) 60, (j) 80, (k) 85, (l) 90, (m) 95, (n) 100%. (b) and (c): Variation of the fluorescence intensity at the maximum emission and the position of the emission band at different ethanol contents. (d) Time dependence of the parietin fluorescence intensity recorded at the maximum of the band at the following ethanol/water contents: (a) 5, (b) 15, (c) 20, (d) 25, (e) 30, (f) 35, (g) 40, (h) 55, (i) 65, (j) 85, (k) 100%.

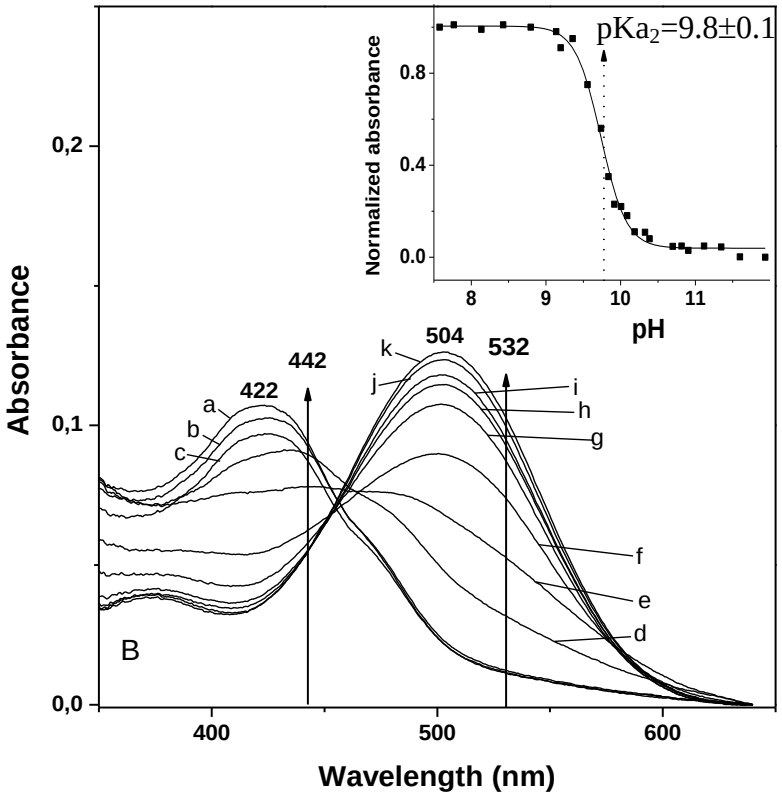

Figure 4

UV-vis absorption spectra of parietin (10^{-5} M) in water–ethanol mixture (5% ethanol) at the following pH: (a) 7.58, (b) 8.13, (c) 8.80, (d) 9.56, (e) 9.73, (f) 9.84, (g) 10.09, (h) 10.19, (i) 10.39, (j) 10.91, (k) 11.94. The vertical dashed arrow shows the increase of the absorbance with increasing the pH. The solid arrow indicates the position of exciting wavelength using in the SERS experiments. Inset: pH titration curve of parietin determined from the normalized values of the absorbance at 504 nm.

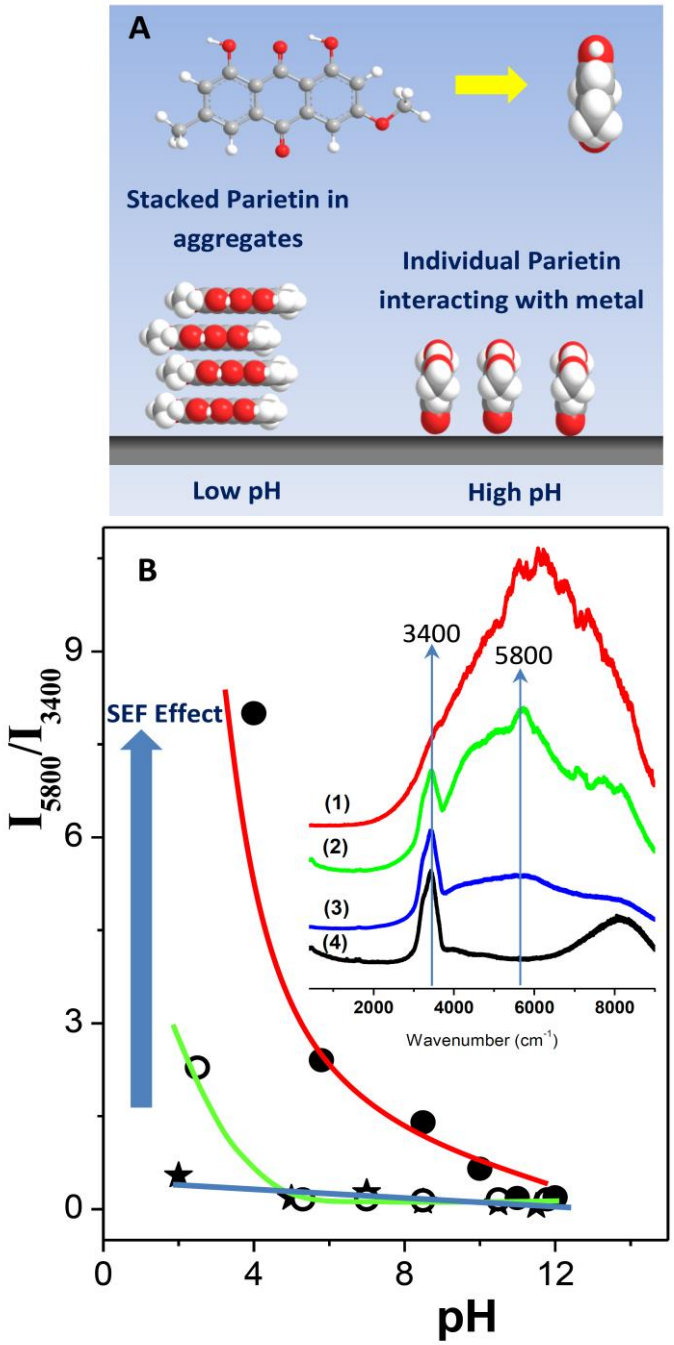

Figure 5

(A): Scheme showing the metal surface adsorption mechanism proposed for parietin at low concentrations by means of molecular aggregates, and by interaction of the individual molecules at high pH. (B) Emission spectra (Fluorescence+Raman) of parietin in different solutions and at different concentrations of parietin: (1) 7×10^{-6} M parietin on Ag NPs at pH 3.9; (2) 5×10^{-7} M parietin on Ag NPs at pH 2.5; (3) 5×10^{-7} M parietin in ethanol/water mixture (5% ethanol) at pH 2.0; and (4) 5×10^{-7} M parietin on Ag NPs at pH 12.2. Plots showing the variation of I_{5800}/I_{3400} with the pH at the following conditions: on Ag NPs at concentrations 7×10^{-6} M (dark circles) and 5×10^{-7} M (open circles) of parietin, and in ethanol/water solution (5%) at concentration 5×10^{-7} M (stars).

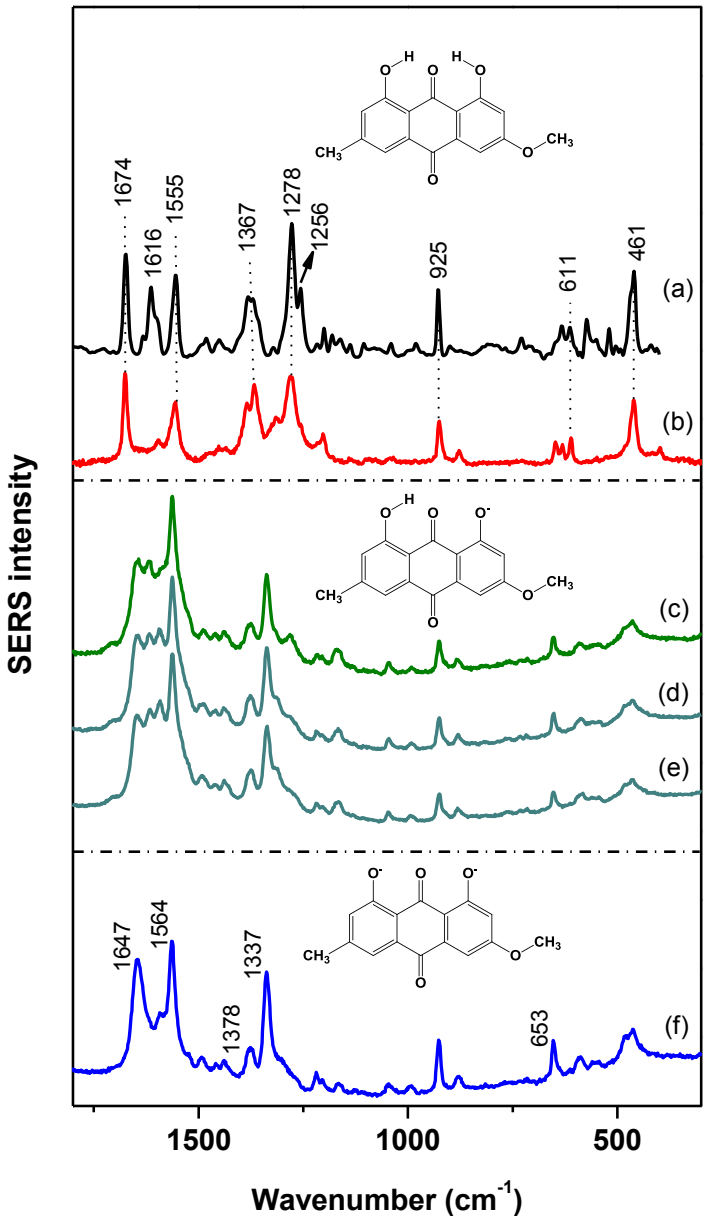

Figure 6

FT-Raman spectrum of the solid parietin obtained using excitation at 1064 nm (a) and SERS spectra of parietin at pH 2.5 (b), 5.5 (c), 6 (d), 8 (e) and 12 (f) corresponding to the three different parietin forms (neutral, monoanionic and dianionic) existing at different pH. All spectra obtained with the excitation line at 442 nm.

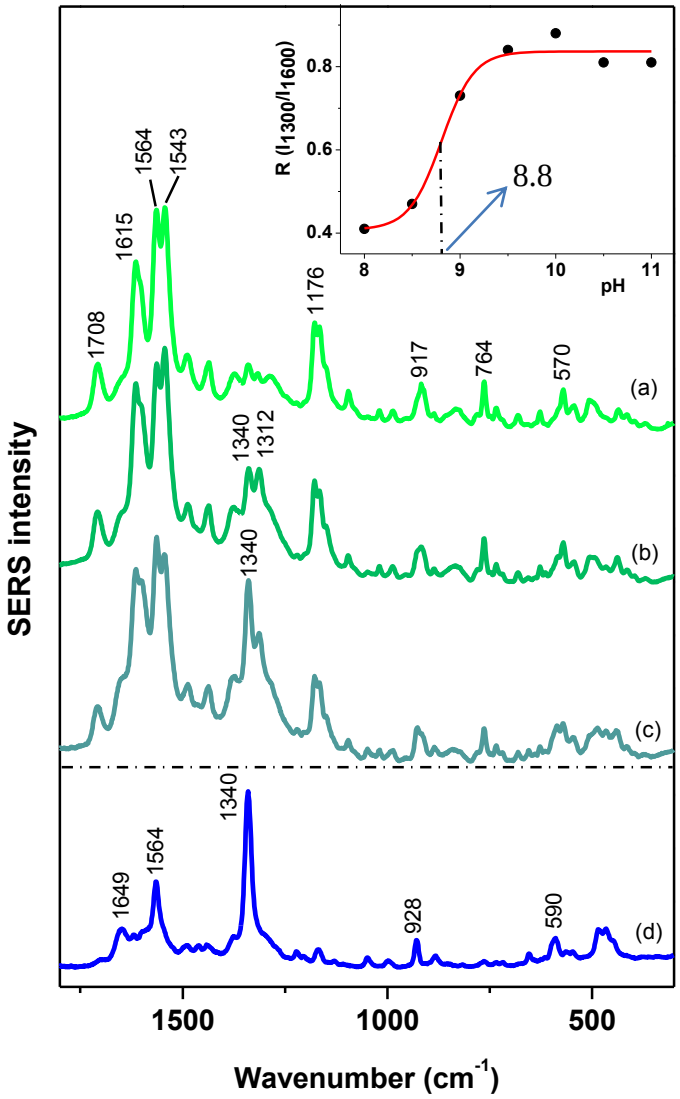

Figure 7

SERS spectra of parietin at pH 5.5 (a), 6 (b), 8 (c) and 12 (d). Inset: Variation of the intensity ratio of the bands appearing in the 1550–1620 cm^{-1} region and those in the 1300–1350 cm^{-1} region and the pKa_2 determination from this variation. All spectra obtained with the excitation line at 532 nm.

Highlights

Surface-enhanced Raman and fluorescence of antitumoral drug parietin

Aggregation of parietin in ethanol/water mixture

Adsorption and aggregation of parietin on plasmonic nanoparticles

Ionization of parietin in solution and when adsorbed on metal nanoparticles

Graphical Abstract